

Image Stitching by Line-guided Local Warping with Global Similarity Constraint

Tianzhu Xiang¹, Gui-Song Xia¹, Xiang Bai², Liangpei Zhang¹

¹*State Key Lab. LIESMARS, Wuhan University, Wuhan, China.*

²*Electronic Information School, Huazhong University of Science and Technology, China.*

June 10, 2022

Abstract

Low-textured image stitching remains a challenging problem. It is difficult to achieve good alignment and is easy to break image structures, due to the insufficient and unreliable point correspondences. Besides, for the viewpoint variations between multiple images, the stitched images suffer from projective distortions. To this end, this paper presents a line-guided local warping with global similarity constraint for image stitching. A two-stage alignment scheme is adopted for good alignment. More precisely, the line correspondence is employed as alignment constraint to guide the accurate estimation of projective warp, then line feature constraints are integrated into mesh-based warping framework to refine the alignment while preserving image structures. To mitigate projective distortions in non-overlapping regions, we combine global similarity constraint with the projective warps via a weight strategy, so that the final warp slowly changes from projective to similarity across the image. This is also integrated into local multiple homographies model for better parallax handling. Our method is evaluated on a series of images and compared with several other methods. Experiments demonstrate that the proposed method provides convincing stitching performance and outperforms other state-of-the-art methods.

1 Introduction

Limited by the narrow field of view (FOV) of cameras, image stitching has been proposed to combine a group of images with overlapping regions to generate a single while larger mosaic with a wider FOV, and has been widely used in many tasks in photogrammetry [1], remote sensing [2] and computer vision [3, 4].

In the literatures [5], to produce image stitching results with satisfied visual effects, there are often two aspects that we can make the effort: (1) developing better alignment models for image stitching, or (2) employing image composition algorithms, such as seam cutting [6], blending [7]. Image alignment is the first and also crucial step in image stitching. Although the advanced image composition methods can relieve stitching artifacts and improve stitching performance, they cannot address obvious misalignments. If the seam or blending areas coincide with the misaligned areas, the image composition schemes may fail to provide a satisfactory stitching of images [8].

Most previous image stitching methods often estimate the global geometric transformations (*e.g.* similarity, affine or projective transformation) that bring the overlapping images into alignment. They require the camera rotation with a fixed projective center, or a limited depth variance in the scenes [9]. These restrictive imaging assumptions are often violated in practice, resulting in artifacts in the stitched images, *e.g.* misalignments or ghosting.

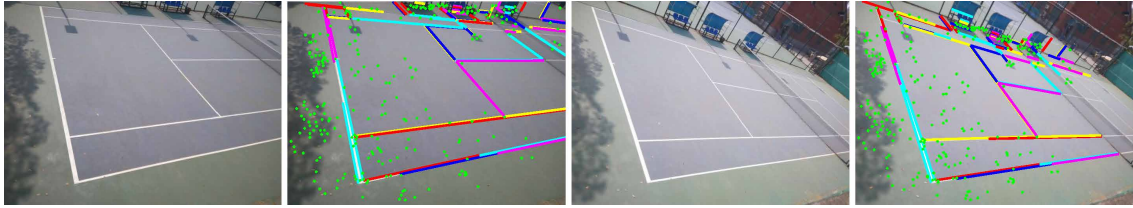
To compensate these geometry assumptions, some spatially-varying warping methods for image stitching have been proposed in recent years. These methods can be roughly categorized into two groups: multiple homographies and mesh-based warping. The former estimates multiple homographies that are compatible with local geometries to align input images, *e.g.* *as-projective-as-possible* (APAP) warp [5]. The latter first pre-warps the image with the global homography, then adopts some energy functions to optimize the alignment as a mesh warping problem, *e.g.* *content preserving warping* (CPW) [10]. With high degrees of freedom (DOFs), these methods can better handle parallax than the global transformations and provide satisfactory stitching results. However, there are still some challenges need to be addressed:

- These methods often fail to achieve satisfactory alignment in low-texture images. Due to the high DOFs, it is inevitable that these methods heavily depend on point correspondences. In some low-texture images, key-points are difficult to be detected because of homogeneous regions, such as indoor walls, sky, artificial structures, thus they are not sufficient and distinctive enough to provide rich and reliable correspondences. Hence, the warping model is often erroneously estimated, which causes misalignments.
- The influence of projective distortions has not been fully considered. As many methods are based on projective transformation, *e.g.* CPW [10], APAP [5], for the images taken under various photographing viewpoints, the stitched results may suffer from projective distortions [11] in the non-overlapping regions, including shape and perspective distortions. For instance, some regions in the stitched image may be stretched or non-uniformly enlarged, and the perspective of each image is difficult to be preserved (Fig. 1 (b), Fig. 7 (a)).
- The distortion of image structures is not fully taken into consideration. Some local warping models, *e.g.* CPW [10], APAP [5], may bend the line structure, especially when stitching the low-texture images. For instance, due to insufficient or unreliable key-points, some local transformations are erroneously estimated in APAP. This makes the local regions misaligned and then causes distortions on the line structures that span multiple local regions. In addition, CPW only employs feature correspondences and content smoothness to optimize the global transformation, without considering the structure constraints.

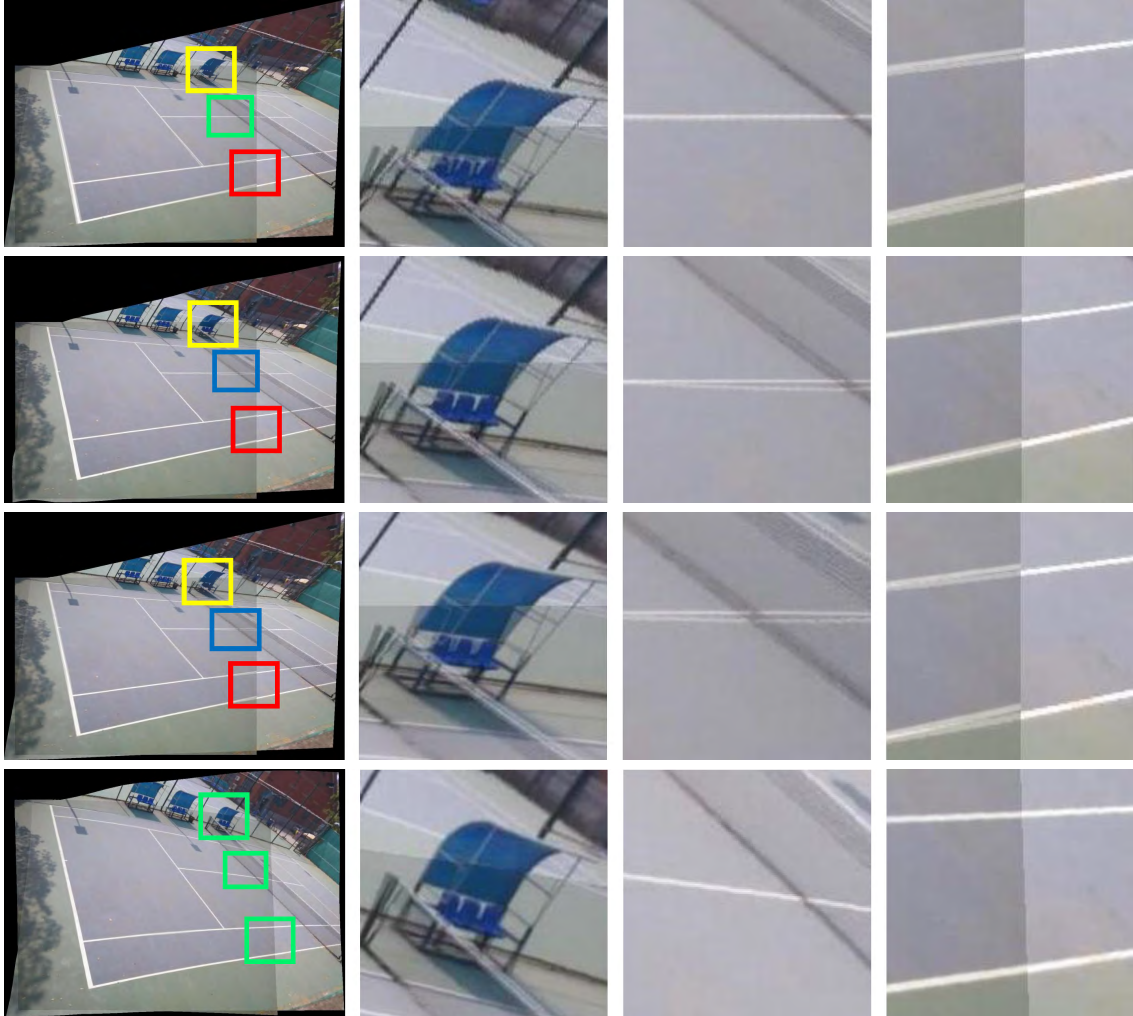
These challenges can be clearly seen in Fig.1. Fig.1 (a) shows the original images and the detected features (points and lines). In some homogeneous regions, only a few points are detected and matched, making it difficult to estimate an accurate transformation. Fig.1 (b) shows the stitching results by the methods of global homography [12], CPW [10], APAP [5] and the proposed method. Violating of the restrictive imaging conditions, the global homography model does not fit for the data, thus it results in obvious misalignments which can be seen in red boxes. In the low-textured areas with insufficient correspondences (in red boxes), CPW lacks data to further align the pre-warping result, and APAP also cannot estimate accurate local homographies, so the misalignments remain obvious. Besides, the lack of point correspondences leads to the structure deformation in CPW and APAP shown in blue boxes, where straight lines are deformed into curves. Due to the projective transformation used in these three models and that no measures taken to eliminate distortions, the stitched images by these methods suffer from severe projective distortions. This can be seen in yellow boxes, where the chairs are enlarged non-uniformly.

The above problems raise a strong motivation for improving the performance of image stitching. To our knowledge, only a few works dedicated to handle the aforementioned one or two problems, so more efforts are still demanded. [13] and [14] have recently presented that line features can be used to improve the performance of alignment. [11] and [15] have recently showed that similarity transformation has advantages in reducing distortions. Inspired by these studies, our work is based on the following two consensus:

- In most man-made environment, the line features are relatively abundant, thus they can be regarded as effective supplement to provide rich correspondences for accurate warping model estimation. What's



(a) The original images and the detected features



(b) Stitching results of global homography, CPW, APAP and our method.

Figure 1: The challenges in image stitching. (a) The original images and the detected features (points & lines). (b) The stitching results. From top to bottom, the results are: global homography [12], CPW [10], APAP [5], and the proposed method. For better comparison, the details are highlighted. Red boxes show alignment errors, yellow boxes show distortions, blue boxes show the deformation of structures, and green boxes show the satisfactory stitching without misalignments or distortions.

more, the line feature depicts the geometrical and structural information of scenes [16, 17], so it can also be used to preserve the image structures.

- Similarity transformation [11] does not introduce shape distortion as it only consists of translation, rotation and uniform scaling. Also it can be regarded as a combination of panning, zooming and in-plane rotation of a camera, so it can preserve the viewing direction.

It is thus of great interest to investigate how to integrate line features and global similarity transformation to improve the performance of image stitching. To this end, this paper presents a line-guided local warping model for image stitching with global similarity constraint. More precisely, this method adopts two-stage scheme to achieve good alignment. First, the pre-warping is estimated jointly by point and line features. Then the extended mesh-based warping is used to further align the pre-warping result. Meantime, line features are integrated into mesh-based warping framework as structural constraints to preserve image structures. Besides, to prevent the undesirable distortions, the global similarity transformation is adopted as similarity constraint to adjust the estimated warping model. The contributions of our work are as follows:

- We introduce the line features to guide the warping estimation, especially in low-texture cases. The line feature plays a significant role mainly in two aspects: providing sufficient and reliable corresponding information for accurate alignment, and imposing multiple constraints (line correspondence and line colinearity) to refine the stitching performance.
- We present a weight integration strategy to combine the global similarity constraint with global homography or multiple homographies model. With this strategy, the resultant warping can achieve smooth transition from projective to similarity across the image, so it can significantly mitigate projective distortions in the non-overlapping regions.
- We propose a robust and effective two-stage stitching framework, which combines local multiple homographies model and mesh-based warping model with line and global similarity constraints. The proposed method can handle local variation well to ensure image alignment by locally stitching and flexible refinement. The method also preserves image structures and multi-perspective by strong geometrical and structural constraints.

The rest of this paper is organized as follows. Section 2 gives a brief review of the related work. Section 3 describes the proposed method in detail. The experimental results and analysis are reported in Section 4. Finally, we draw some conclusions and remarks in Section 5.

2 Related work

Tremendous studies have been devoted to image stitching, a comprehensive survey of which can be found in [9]. The global homography model [12] works well for planar scenes or parallax free camera motion, but violation of these assumptions may lead to ghosting artifacts.

Recently, spatially-varying warping methods have been proposed to handle parallax flexibly. Liu *et al.* [10] proposed the *content preserving warping* (CPW) which was first used in video stabilization. CPW adopts registration error and content smoothness to refine the pre-warping result obtained by the global homography. A simple extension of global homography method was presented in [18], called *dual-homography warping* (DHW), which divides the whole scene into two planes: a distant plane and a ground plane. The final warping is obtained by the linear combination of these two homographies estimated by point correspondences of each plane. But it is difficult to handle complex scenes. Lin *et al.* [19] proposed the *smoothly varying affine* (SVA) warping for image stitching, which can handle local deformations while preserving global affinity. However because of insufficient DOFs of affine model, SVA cannot achieve projective warping. Zaragoza *et*

al. [5] extended the previous method and proposed an *as-projective-as-possible* (APAP) warping for image stitching, which achieves a smoothly varying projective stitching field estimated by moving direct linear transformation (DLT) [20]. It maintains globally projective and allows local non-projective deviations. Zhang *et al.* [3] proposed a parallax-tolerant image stitching method. The method seeks for the optimal homography evaluated by the seam cost, and further uses CPW to refine the alignment. However, these methods are based on projective transformation except SVA, thus the stitched images often suffer from projective distortions. In addition, the resulting images may suffer from structure deformations because of the nonlinear local transformations in the model.

In recent years, similarity transformation has been introduced to reduce the distortions. Chang *et al.* [11] proposed a *shape-preserving half-projective* (SPHP) warping for image stitching, which adopts projective, transition and similarity transformation to achieve gradually change from projective to similarity across the image. It can significantly reduce the distortions and preserve the image shape. But it may introduce structure deformations, *e.g.* line distortions, when the scene is dominated by line structures. Lin *et al.* [15] proposed an *adaptive as-natural-as-possible* (AANAP) warping, which linearizes the homography in the non-overlapping regions and combines these homographies with global similarity transformation by the direct and simple distance-based weight strategy to mitigate the perspective distortion. However, some distortions locally still exist when stitching images (Fig. 12(b)).

It is worth noting that the above mentioned methods greatly depend on point correspondences. If there is no sufficient and reliable points, such as low-texture images, the estimated model will lose their effect. More recently, Joo *et al.* [13] first introduced the line correspondences into local warping model, but it needs user’s annotations of the straight lines, and the parameter setting is complex. Li *et al.* [14] proposed a dual-feature warping for motion model estimation, which combines line segments and points to estimate the global homography. However it still suffers from projective distortions.

3 The proposed approach

This section introduces the proposed method for image stitching in detail. The main idea is to integrate line constraints and global similarity constraint into a two-stage alignment framework. The outline of our method is given in Fig. 2. The first-stage alignment (presented in Section 3.1) is to estimate the accurate warping model under the line guidance. Line features are adopted as an alignment constraint to jointly estimate global or local homography with point correspondences, which provides rich and reliable correspondences in low-texture images. To further improve alignment, we extend the content preserving warping framework, presented in Section 3.2. Line feature constraints, *i.e.* line correspondence and line colinearity, are combined into the CPW framework to further refine the alignment and also preserve the image structures. Then, in order to mitigate projective distortions, global similarity transformation is employed to integrate into the warping model estimated in the first-stage via a reasonable weight strategy (Section 3.3). Based on the proposed warping model, we finally able to achieve accurate and distortion-free image stitching.

3.1 Line-guided warping model

Given the target and reference images $I, I': \mathbb{R} \times \mathbb{R} \mapsto \mathbb{R}$, and a pair of matching points: $\mathbf{p} = [x, y, 1]$, $\mathbf{p}' = [x', y', 1]$ with $x, y \in \mathbb{R}$ represented by homogeneous vectors between I and I' . The global homography $\mathbf{H} \in \mathbb{R}^{3 \times 3}$ that maps \mathbf{p} to \mathbf{p}' satisfies: $\mathbf{p}' = \mathbf{H}\mathbf{p}$. Through direct linear transformation, it can be rewritten as a cross product: $\mathbf{p}' \times \mathbf{H}\mathbf{p} = \mathbf{0}_{3 \times 1}$. The homography can be estimated by minimizing the algebraic distance: $\sum_i \left\| \mathbf{p}'_i \times \mathbf{H}\mathbf{p}_i \right\|^2$ with a set of matching points, where i is the index of matching points.

However, as stated previously, key-points extracted from images are very limited in some textureless scenarios, thus it is difficult to estimate an accurate global homography for image stitching. Hence, we resort

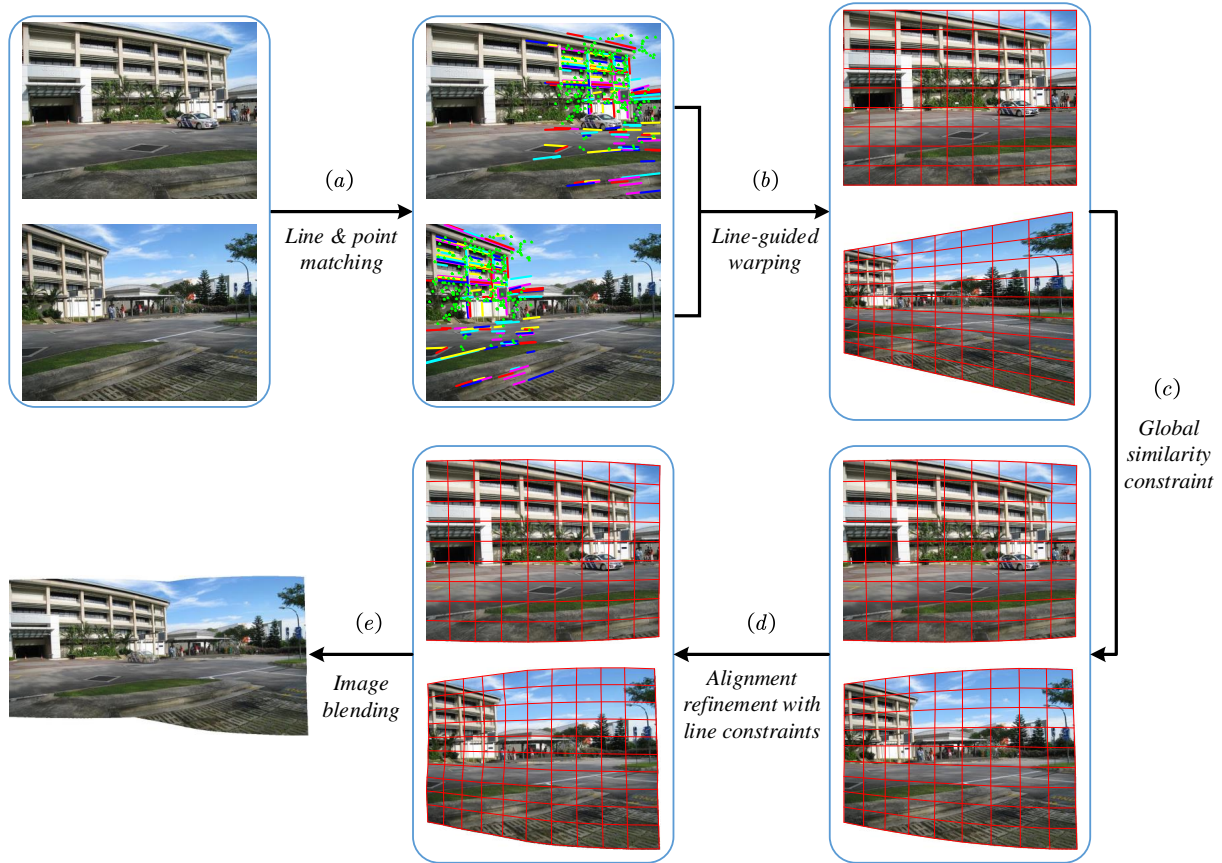


Figure 2: The flowchart of the proposed approach. (a) feature matching, (b) line-guided warping, (c) distortion reduction by global similarity constraint, (d) alignment refinement with line constraints, (e) image blending.

to the line features, which are salient in artificial scenarios. The line correspondences can be regarded as the alignment constraint to guide the global homography estimation.

Let $\mathbf{l} = [a, b, c]^T$, $\mathbf{l}' = [a', b', c']^T$, with $a, b, c \in \mathbb{R}$ be a pair of matching lines in target and reference images respectively. The $\mathbf{p}^{0,1} = [x^{0,1}, y^{0,1}, 1]$ denotes two endpoints of line \mathbf{l} . This pair of matching lines satisfy: $\mathbf{l}'^T \mathbf{H} \mathbf{p}^{0,1} = 0$, which means that the endpoints transformed by \mathbf{H} from \mathbf{l} should lie on its corresponding line \mathbf{l}' . So \mathbf{H} can be estimated by minimizing the algebraic distance: $\sum_j \|\mathbf{l}'^T \times \mathbf{H} \mathbf{p}_j^{0,1}\|^2$ with a set of matching lines, where j is the index of matching lines.

The homography can be then estimated jointly by point and line correspondences:

$$\begin{aligned}
 \hat{\mathbf{h}} &= \arg \min_{\mathbf{h}} \left(\sum_i \|\mathbf{p}'_i \times \mathbf{H} \mathbf{p}_i\|^2 + \sum_j \|\mathbf{l}'^T_j \times \mathbf{H} \mathbf{p}_j^{0,1}\|^2 \right) \\
 &= \arg \min_{\mathbf{h}} \left(\sum_i \|\mathbf{A}_i \mathbf{h}\|^2 + \sum_j \|\mathbf{B}_j \mathbf{h}\|^2 \right), \quad s.t. \|\mathbf{h}\| = 1,
 \end{aligned} \tag{1}$$

where $\mathbf{h} = [h_1, h_2, h_3, h_4, h_5, h_6, h_7, h_8, h_9]$ is the column vector representation of \mathbf{H} , $\mathbf{A}_i, \mathbf{B}_j \in \mathbb{R}^{2 \times 9}$ are the coefficient matrix computed by the i -th matching point and j -th matching line, respectively. Note that

$\mathbf{A}_i \in \mathbb{R}^{2 \times 9}$, because only two rows of the coefficient matrix are independent.

$$\mathbf{A}_i = \begin{bmatrix} x_i & y_i & 1 & 0 & 0 & 0 & -x'_i x_i & -x'_i y_i & -x'_i \\ 0 & 0 & 0 & x_i & y_i & 1 & -y_i x_i & -y_i y_i & -y_i \end{bmatrix}, \quad (2)$$

$$\mathbf{B}_j = \kappa_j \begin{bmatrix} a'_j x_j^0 & a'_j y_j^0 & a'_j & b'_j x_j^0 & b'_j y_j^0 & b'_j & c'_j x_j^0 & c'_j y_j^0 & c'_j \\ a_j x_j^1 & a_j y_j^1 & a_j & b_j x_j^1 & b_j y_j^1 & b_j & c_j x_j^1 & c_j y_j^1 & c_j \end{bmatrix}, \quad (3)$$

where κ_j is a scale parameter for balancing with \mathbf{A}_i , and $\kappa_j = 1/\sqrt{a_j'^2 + b_j'^2}$.

Stacking vertically all the coefficient matrices of points (\mathbf{A}_i) and lines (\mathbf{B}_j) into a unified matrix: $\mathbf{C} = [\mathbf{A}; \mathbf{B}]$, $\mathbf{C} \in \mathbb{R}^{2(N+M) \times 9}$, where N and M are the number of point and line correspondences respectively, the Eq.(1) can be rewritten as

$$\hat{\mathbf{h}} = \arg \min_{\mathbf{h}} \|\mathbf{C}\mathbf{h}\|^2, \quad s.t. \|\mathbf{h}\| = 1, \quad (4)$$

The global homography \mathbf{H} is the smallest significant right singular vector of \mathbf{C} . Note that before estimation, all the entries of stacked matrices $[A_i; B_j]$ should be normalized for numerical stability. In our case, the point-centric normalization approach proposed in [21] is adopted.

According to [5], local homography can handle parallax better than global homography due to the higher DOFs. Therefore, we extend the line-guided global homography to local homographies. The input images are first divided into uniform grid mesh. The local homography \mathbf{h}_k of k -th mesh located at $\mathbf{p}_* = [x_*, y_*]$ is estimated by:

$$\mathbf{h}_k = \arg \min_{\mathbf{h}} \|\mathbf{W}_k \mathbf{C}\mathbf{h}\|^2, \quad s.t. \|\mathbf{h}\| = 1, \quad (5)$$

where $\mathbf{W}_k = \text{diag}([\mathbf{w}^p, \mathbf{w}^l])$, $\mathbf{w}^p \in \mathbb{R}^{2N}$ and $\mathbf{w}^l \in \mathbb{R}^{2M}$ denote weight factors of point and line correspondences, respectively. Specifically, $\mathbf{w}^p = [w^{p_1} w^{p_1} \dots w^{p_N} w^{p_N}]$, $\mathbf{w}^l = [w^{l_1} w^{l_1} \dots w^{l_M} w^{l_M}]$. So the solution is the smallest significant right singular vector of $\mathbf{W}\mathbf{C}$.

The point weight factor \mathbf{w}^p is calculated by Gaussian weighted Euclidean distance,

$$\mathbf{w}^{p_i} = \max \left(\exp \left(-\|\mathbf{p}_* - \mathbf{p}_i\|^2 / \sigma^2 \right), \eta \right), \quad (6)$$

where \mathbf{p}_i is the i -th key-point, σ is the scale parameter, and $\eta \in [0, 1]$ is used to avoid the numerical issues caused by the small weights when the mesh center \mathbf{p}_* is far away from key-point \mathbf{p}_i , as shown in Fig. 3 (a).

The line weight factor \mathbf{w}^l is calculated as:

$$\mathbf{w}^{l_j} = \max \left(\exp \left(-d_l(\mathbf{p}_*, \mathbf{l}_j)^2 / \sigma^2 \right), \eta \right), \quad (7)$$

where $d_l(\mathbf{p}_*, \mathbf{l}_j)$ is the shortest distance between mesh center \mathbf{p}_* and line \mathbf{l}_j .

$$d_l(\mathbf{p}_*, \mathbf{l}_j) = \begin{cases} \min(\|\mathbf{p}_* - \mathbf{p}_j^0\|, \|\mathbf{p}_* - \mathbf{p}_j^1\|) & (a) \\ |a_j x_* + b_j y_* + c_j| / \sqrt{a_j^2 + b_j^2} & (b) \end{cases}, \quad (8)$$

where $\mathbf{p}_j^0, \mathbf{p}_j^1$ are the endpoints of line $\mathbf{l}_j : \mathbf{l}_j = [a_j, b_j, c_j]$. As shown in Fig. 3 (b), if \mathbf{p}_* is in the R_1 or R_2 region, the d_l is calculated by (a), and if \mathbf{p}_* is in the R_3 region, d_l is calculated by (b). From Eq.(6) and (7), the weight is higher when the key-point or line is closer to mesh center \mathbf{p}_* , which makes the local homography better fit for the local structure around \mathbf{p}_* .

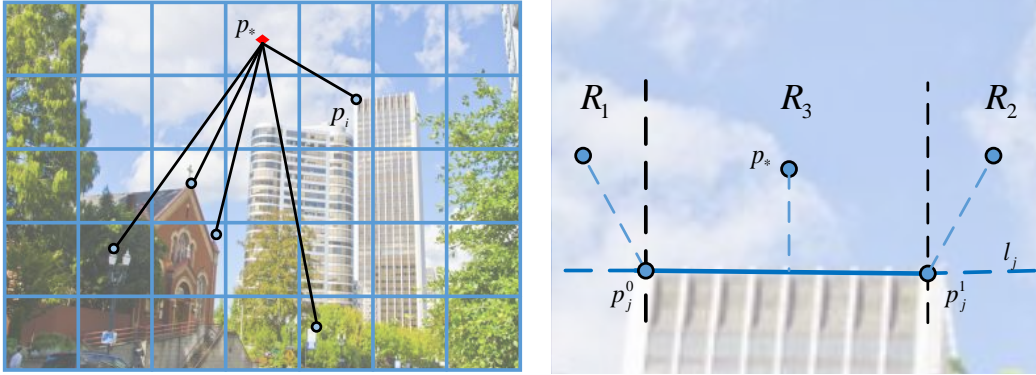


Figure 3: Weight computation of point & line. Left: (a) The distance between mesh center \mathbf{p}_* and key-point \mathbf{p}_i . Right: (b) The distance between mesh center \mathbf{p}_* and line segment \mathbf{l}_j .

3.2 Alignment refinement with line constraints

In this section, we adopt the content-preserving warping framework as the second step of the two-stage alignment scheme to further improve the performance of image stitching. Content preserving warping is one of the mesh-based warping methods, which was first used in video stabilization [10] and then successfully applied in image stitching [22–24]. It is well suited for small local adjustment. In our work, the content-preserving warping framework is extended with line feature constraints, *e.g.* line correspondence constraint and line collinearity constraint, so that it can well maintain the image structures as well as refine the alignment.

The target image I is first divided into regular grid mesh. In our case, the grid mesh is used to guide the image warping. Supposing $\bar{\mathbf{V}}$ denotes the vertices of grid mesh in the pre-warping image transformed by line-guided warping model. Alignment refinement is to find a group of deformed vertices \mathbf{V} by energy optimization. For arbitrary point \mathbf{p} in pre-warping image, it can be represented by a linear combination of four mesh vertices $\mathbf{V} = [\mathbf{V}_1, \mathbf{V}_2, \mathbf{V}_3, \mathbf{V}_4]^T$ in its locating quad: $\mathbf{p} = \mathbf{w}^T \mathbf{V}$, and $\mathbf{w} = [w_1, w_2, w_3, w_4]^T$ is calculated by the inverse bilinear interpolation [25] and sum to 1. So the image warping problem can be formulated as a mesh warping problem. In fact, it is an optimization problem aiming to accurately align pre-warping image to the reference image and avoid obvious distortions. The energy terms in this paper are detailed below.

3.2.1 Content preserving warping

Content preserving warping [22] terms include three energy terms: point alignment term, global alignment term and smoothness term.

Point alignment term E_p is used to align the feature points in the target image or pre-warping image to the corresponding points in the reference image as much as possible, and defined as

$$E_p = \sum_i \left\| \mathbf{w}_i^T \mathbf{V}_i - \mathbf{p}'_i \right\|^2, \quad (9)$$

where \mathbf{p}'_i is the matching point in the reference image. This term ensures the alignment of overlapping region.

Global alignment term E_g is used to constraint the image regions without feature correspondences to be consistent with the pre-warping result as much as possible.

$$E_g = \sum_i \left\| \mathbf{V}_i - \bar{\mathbf{V}}_i \right\|^2, \quad (10)$$

where $\bar{\mathbf{V}}_i$ is the corresponding vertex in the pre-warping result.

Smoothness term E_s encourages each grid in the pre-warping result to preserve similarity during warping to avoid shape distortions as much as possible. Precisely, given a triangle $\Delta \bar{\mathbf{V}}_0 \bar{\mathbf{V}}_1 \bar{\mathbf{V}}_2$ in the pre-warping result, the vertex $\bar{\mathbf{V}}_0$ can be represented by $\bar{\mathbf{V}}_1$ and $\bar{\mathbf{V}}_2$,

$$\bar{\mathbf{V}}_1 = \bar{\mathbf{V}}_2 + \mu(\bar{\mathbf{V}}_3 - \bar{\mathbf{V}}_2) + \nu \mathbf{R}(\bar{\mathbf{V}}_3 - \bar{\mathbf{V}}_2), \quad \mathbf{R} = \begin{bmatrix} 0 & 1 \\ -1 & 0 \end{bmatrix}, \quad (11)$$

where μ, ν are the coordinate value of $\bar{\mathbf{V}}_0$ in the coordinated system defined by the other two vertices. During warping, the triangle takes a similarity transformation to preserve the relative relationship of three vertices and avoid the local distortions. The smoothness term is

$$E_s(\mathbf{V}_1) = \varphi \|\mathbf{V}_1 - (\mathbf{V}_2 + \mu(\mathbf{V}_3 - \mathbf{V}_2) + \nu \mathbf{R}(\mathbf{V}_3 - \mathbf{V}_2))\|^2, \quad (12)$$

where φ is a weight used to measure the salience of triangle using the same method as [10]. The weight is to preserve the shape of salient regions stronger than low salient regions. The full smoothness energy term is formed by summing Eq. (12) over all the vertices.

3.2.2 Line correspondence term

Content preserving warping terms only ensure the point alignment in the overlapping regions, thus the line correspondences are taken into consideration to further improve the alignment.

Line correspondence term is utilized to ensure the line correspondences are well aligned. Let $\mathbf{l}_j, \mathbf{l}'_j$ be a pair of line correspondences in the target and reference images respectively. Line \mathbf{l}_j is cut into several short line segments by the edges of mesh if the line \mathbf{l}_j goes across this mesh. The endpoints of short line segments from \mathbf{l}_j are denoted by $\mathbf{p}_{j,k}$, where k is the index of endpoints. $\mathbf{p}'_{j,k}$ denotes the endpoints in pre-warping image transformed from $\mathbf{p}_{j,k}$ by the foregoing warping, $\mathbf{p}'_{j,k} = \mathbf{w}_{j,k}^T \mathbf{V}_{j,k}$. The line correspondence term can be expressed as the distance from $\mathbf{p}'_{j,k}$ to the corresponding line \mathbf{l}'_j should be the minimum.

$$E_l = \sum_{j,k} \left\| (\mathbf{l}'_j)^T \cdot \mathbf{w}_{j,k}^T \mathbf{V}_{j,k} / \sqrt{a_j'^2 + b_j'^2} \right\|^2. \quad (13)$$

The line correspondence term not only enhances the image alignment but also preserves the straightness property of line structures, together with line collinearity term below.

3.2.3 Line collinearity term

The above terms may not reduce the distortions, *e.g.* line structure distortion, in the non-overlapping regions where there are few point or line correspondences. To make use of line features and preserve the line structure, the line collinearity constraint is adopted.

Line collinearity term is used to preserve the straightness of line structures of the target image as much as possible. Let $\mathbf{p}_{i,k}$ denote the endpoints and intersection points of line \mathbf{l}_i in the non-overlapping regions with the grid. Supposing $\mathbf{p}'_{i,k}$ is the corresponding points of $\mathbf{p}_{i,k}$ in the pre-warping result. The line should maintain straightness when warping, that is, the transformed points $\mathbf{p}'_{i,k}$ should lie on the same line. This can be represented by the distance from endpoints $\mathbf{p}'_{i,k}$ to the line $\hat{\mathbf{l}}_i$ which should be the minimum. Line $\hat{\mathbf{l}}_i$ is calculated by the head and tail endpoints of $\mathbf{p}'_{i,k}$. The term is defined as

$$E_c = \sum_{i,k} \left\| (\hat{\mathbf{l}}_i)^T \cdot \mathbf{w}_{i,k}^T \mathbf{V}_{i,k} / \sqrt{\hat{a}_i^2 + \hat{b}_i^2} \right\|^2. \quad (14)$$

The line collinearity term maintains the line structures well, together with line correspondence term.

3.2.4 Objective function

The above five energy terms are then combined as an energy optimization problem, the objective function is:

$$E = \alpha E_p + \beta E_g + \gamma E_s + \delta E_l + \rho E_c, \quad (15)$$

where α , β , γ , δ , ρ are weight factors of each energy term. The above function is quadratic, so it can be solved by sparse linear solver. The final result is obtained through texture mapping.

3.3 Distortion reduction by global similarity constraint

To reduce the projective distortions in the non-overlapping regions, the global similarity transformation is adopted to adjust the local warping model.

Chang *et al.* [11] has shown that similarity transformation is effective for mitigating distortions. If we can find the similarity transformation which can represent the camera motion of image projection plane approximately, it can be utilized to offset the camera motion. According to [15], RANSAC [26] is used to iteratively segment the matching points. Each group of point correspondences can estimate a similarity transformation. The one with the smallest rotation angle is chosen as the optimal candidate [27]. As shown in Fig. 4, the group of points with green color is chosen to estimate global similarity transformation. We can also see the plane comprised of green points approximates the image projection plane, because the camera is near upright to ground when shooting.

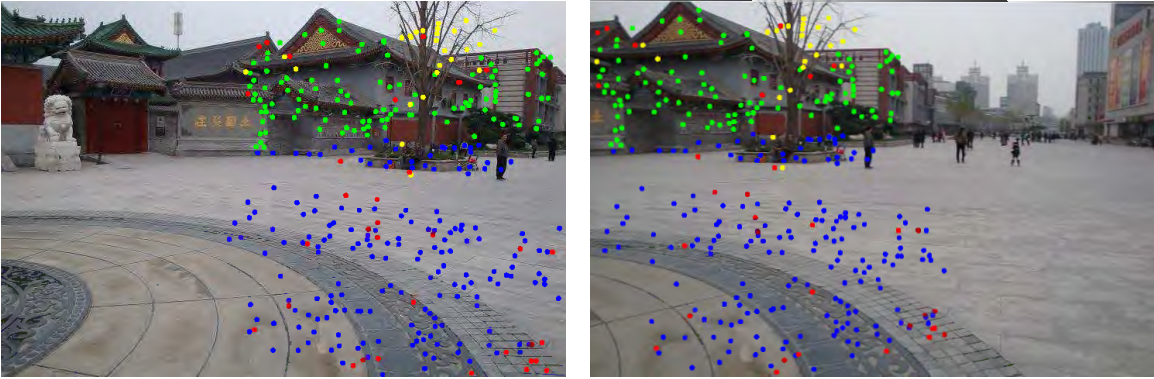


Figure 4: The optimal point correspondences for global similarity transformation estimation.

3.3.1 Similarity constraint

The global similarity transformation is combined with the global or local homographies by weight factor. For smooth transition, the whole image is taken into consideration. The weight integration is calculated as

$$\mathbf{H}'_i = \tau \mathbf{H}_i + \xi \mathbf{S}, \quad (16)$$

where \mathbf{H}_i is the homography in i -th grid mesh, and \mathbf{H}'_i is the final homography in i -th grid mesh. \mathbf{S} is the similarity transformation. α and β are weight coefficients with $\alpha + \beta = 1$. For global homography model, the homography of every grid mesh is the same.

The corresponding warping should also be applied for the reference image, since the similarity transformation also adjust the overlapping regions. The warping for the reference image can be formulated as

$$\mathbf{T}'_i = \mathbf{H}'_i \mathbf{H}_i^{-1}, \quad (17)$$

where \mathbf{T}'_i is the warping for the reference image in the i -th grid mesh.

As shown in Fig. 5, if the point is far from the overlapping regions, especially the distorted non-overlapping regions, it assigns a high weight for similarity transformation so that it can mitigate the distortions as much as possible, while for the point near the overlapping regions, it assigns a high weight for the homography so as to ensure the accuracy of alignment. With the weight combination, the final warping smoothly changes from projective to similarity across the image, so that it can preserve the image shape and multi-perspective.

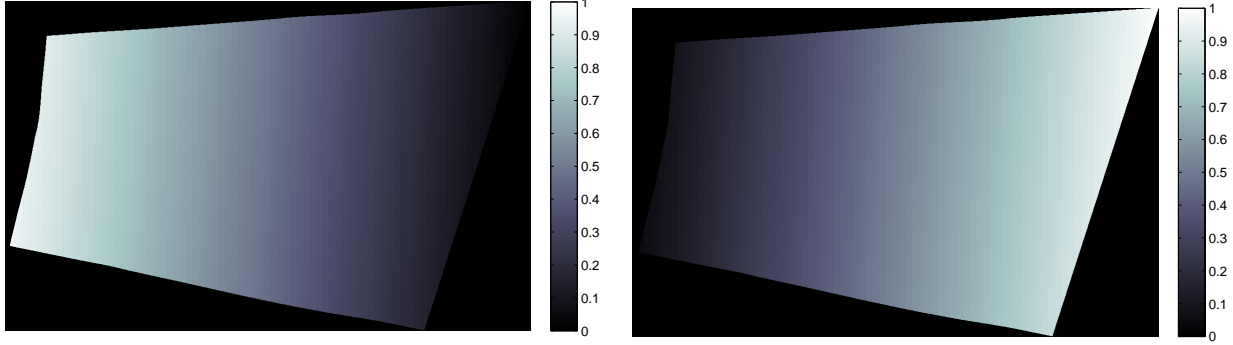


Figure 5: Weight map of the target image in Fig.7. Left: weight map of homography. Right: weight map of global similarity transformation. The color denotes the weight value.

3.3.2 Weighting strategy

The calculation of weight coefficients comes from the analysis of projective transformation. According to [28], let \mathbf{R} be a rotation transformation that transforms the image coordinate (x, y) to a new coordinate (u, v) . Based on $\mathbf{p}' = \mathbf{H}\mathbf{p}$, a new projective transformation \mathbf{Q} that transform (u, v) to (x', y') meets: $\mathbf{p}' = \mathbf{Q}[u, v, 1]^T = \mathbf{H}\mathbf{R}[u, v, 1]^T$, where $\mathbf{H} = [h_1, h_2, h_3; h_4, h_5, h_6; h_7, h_8, 1]$, $\mathbf{Q} = [q_1, q_2, q_3; q_4, q_5, q_6; q_7, q_8, 1]$.

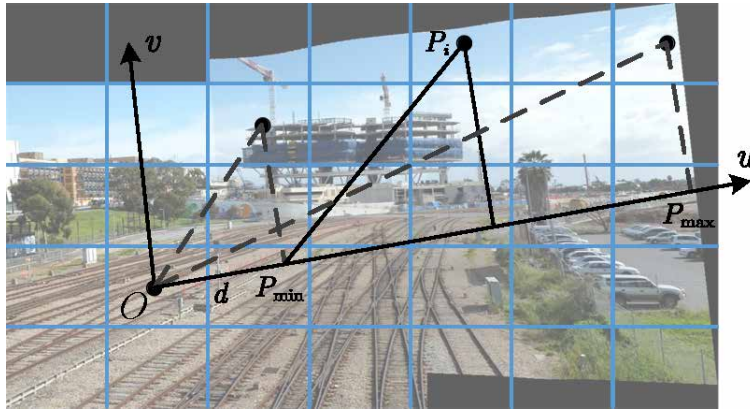


Figure 6: Weight strategy for global similarity transformation and homography.

Supposing the rotation angle $\theta = \arctan(h_8/h_7)$, we can obtain: $q_8 = -h_7 \sin \theta + h_8 \cos \theta = 0$. Then \mathbf{Q}

can be decomposed as:

$$\begin{bmatrix} q_1 & q_2 & q_3 \\ q_4 & q_5 & q_6 \\ -c & 0 & 1 \end{bmatrix} = \underbrace{\begin{bmatrix} q_1 + cq_3 & q_2 & q_3 \\ q_4 + cq_6 & q_5 & q_6 \\ 0 & 0 & 1 \end{bmatrix}}_{\mathbf{Q}_a} \underbrace{\begin{bmatrix} 1 & 0 & 0 \\ 0 & 1 & 0 \\ -c & 0 & 1 \end{bmatrix}}_{\mathbf{Q}_p}, \quad (18)$$

where $c = \sqrt{h_7^2 + h_8^2}$, \mathbf{Q}_a is the affine transformation, and \mathbf{Q}_p is the projective transformation. According to [29], defining the local scale change at point (u, v) under the projective transformation as the determinant of the Jacobian of \mathbf{Q} at point (u, v) , the local scale change is calculated as:

$$\det \mathbf{J}(u, v) = \det \mathbf{J}_a(u, v) \cdot \det \mathbf{J}_p(u, v) = \lambda_a \cdot \frac{1}{(1 - cu)^3}, \quad (19)$$

where \det denotes the determinant, and λ_a is independent of u and v . It can be seen: the local area change derived from \mathbf{Q} only relies on u . In other words, the distortions of projective transformation only occurs along the u -axis. Therefore, in our case, the weight coefficients are calculated in (u, v) coordinate.

As shown in Fig. 6, the centre of reference image is used as the origin of coordination o , and the unit vector on u -axis denotes $\vec{o}\vec{u} = (1, 0)$. For the arbitrary mesh center \mathbf{p} , d is the projected length of vector $\vec{o}\vec{\mathbf{p}}$ on the vector $\vec{o}\vec{u}$. The projected point \mathbf{p}_{max} with maximum length of d and the projected point \mathbf{p}_{min} with minimum length of d can be calculated. For the i -th grid, the weight coefficients are calculated as:

$$\xi = \frac{\langle \vec{o}\vec{\mathbf{p}}_{min} \cdot \vec{o}\vec{\mathbf{p}}_{max} \rangle}{|\vec{o}\vec{\mathbf{p}}_{min}\vec{\mathbf{p}}_{max}|}, \quad (20)$$

where $\langle \vec{o}\vec{\mathbf{p}}_{min} \cdot \vec{o}\vec{\mathbf{p}}_{max} \rangle$ denotes the projection length of $\vec{o}\vec{\mathbf{p}}_{min}$ on $\vec{o}\vec{\mathbf{p}}_{max}$, and $\tau = 1 - \xi$.

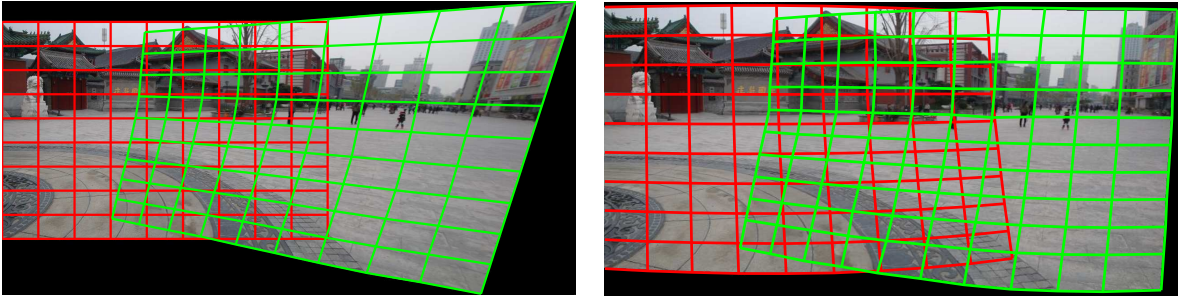


Figure 7: Performance of similarity constraint to reduce projective distortions.

As shown in Fig. 7, APAP adopts the local homographies for alignment, which aims to be globally projective and also allows local deviations. However, the stitched image suffers from projective distortions, for instance, the buildings are undesirably stretched and not parallel to temples, in addition, the perspective distortion in the non-overlapping regions is obvious. With global similarity constraint, the proposed warping model preserves the shape of objects and maintains the perspective of each image.

4 Experimental results and analysis

In this section, several experiments are conducted to assess the performance of the proposed method on a series of challenging images. In our experiments, the testing images are taken casually which corresponding views differ by more than a pure rotation.

Given a pair of input images, the key-points are detected and matched by SIFT [30] in VLFeat library [31]. The line features are detected by line segment detector (LSD) [32] and matched by line-point invariants [33] or line-junction-line [34]. Then RANSAC is used to remove the mismatches, and the remaining inliers are given to the stitching algorithms. We compare our approach with several other methods, and the parameters of other methods are set as the same suggested in the respective papers. We use the code provided by the authors of the papers to obtain the results for comparison. For our method, σ is 8.5, η is 0.01, and the weight factors of energy terms $\alpha, \beta, \gamma, \delta, \rho$ are 1, 0.001, 0.01, 1, 0.001, respectively.

To better compare the methods and reduce the interference, the post-processing methods like blending or seam cutting detailed in [9] are avoided. The aligned images are simply blended by intensity average so that any misalignments remain obvious.

To assess the alignment accuracy of image stitching quantitatively, the correlation (Cor) [15] and mean geometric error (Err_{mg}) [13] are adopted. Cor is defined as one minus *normalized cross correlation* (NCC) over a neighborhood of 3×3 window, that is

$$Cor(I, I') = \sqrt{\frac{1}{N} \sum_{\pi} (1 - NCC(\mathbf{p}, \mathbf{p}'))^2}, \quad (21)$$

where N is the number of pixels in overlapping region π , \mathbf{p} and \mathbf{p}' are the pixels in image I and I' respectively. Cor shows the similarity of two images in the overlapping regions. The smaller the Cor is, the better the stitching result is.

Err_{mg} is defined as the mean geometric error on point and line, that is

$$\begin{aligned} Err_{mg}^{(p)} &= \frac{1}{M} \sum_{i=1}^M \|f(\mathbf{p}_i) - \mathbf{p}'_i\| \\ Err_{mg}^{(l)} &= \frac{1}{2K} \sum_{j=1}^K \sum_{i=0}^1 d_l(f(\mathbf{p}_{l_j}^i), \mathbf{l}'_j) \quad , \\ Err_{mg} &= (Err_{mg}^{(p)} * M + Err_{mg}^{(l)} * 2K) / (M + 2K) \end{aligned} \quad (22)$$

where $f: \mathbb{R}^2 \mapsto \mathbb{R}^2$ is the estimated warping, M is the number of point correspondences, \mathbf{p}_i and \mathbf{p}'_i are a pair of point correspondences, K is the number of line correspondences, d_l denotes the projected distance of endpoints of \mathbf{l}_j to its correspondence line \mathbf{l}'_j . The smaller Err_{mg} means the better stitching result.

In the following subsections, we first verify the performance of the proposed method on image alignment and distortion reduction. Then we report the experimental comparison results including the comparison with the global-based methods and the local-based methods.

4.1 Image alignment

Fig. 8 illustrates the performance of each constraint in the proposed method, including line-guided local warping estimation, line correspondence constraint and line collinearity constraint. Fig. 8(b) shows the result of line-guided warping combined with APAP (LAPAP), which alignment has been largely improved compared with APAP, as can be clearly seen in green and blue boxes. However, LAPAP brings about structure distortions, *e.g.* the bending lines on buildings shown in the red circle of blue box. With point alignment constraint, LAPAP+CPW refines the alignment performance, but it remains slight errors (Fig. 8(c)). Combined with line correspondence (LineCorr) constraint, LAPAP+CPW+LineCorr provides good alignment (Fig. 8(d)). While the structure distortion is not handled gracefully in CPW constraints and line correspondence constraint. With line collinearity constraint to restrain the structure deformation, the proposed method provides a good stitching result with less distortion in this example (Fig. 8(e)). The quantitative evaluation on Cor and Err_{mg} are shown in Table 1, which demonstrate consistent conclusions with visual effect.

Then the proposed method is compared against other flexible warping methods to evaluate the alignment performance, namely, global homography (baseline) [12], CPW [10], APAP [5]. For completeness, the proposed method is also compared with the Image Composite Editor (ICE) [35] (one of the common commercial

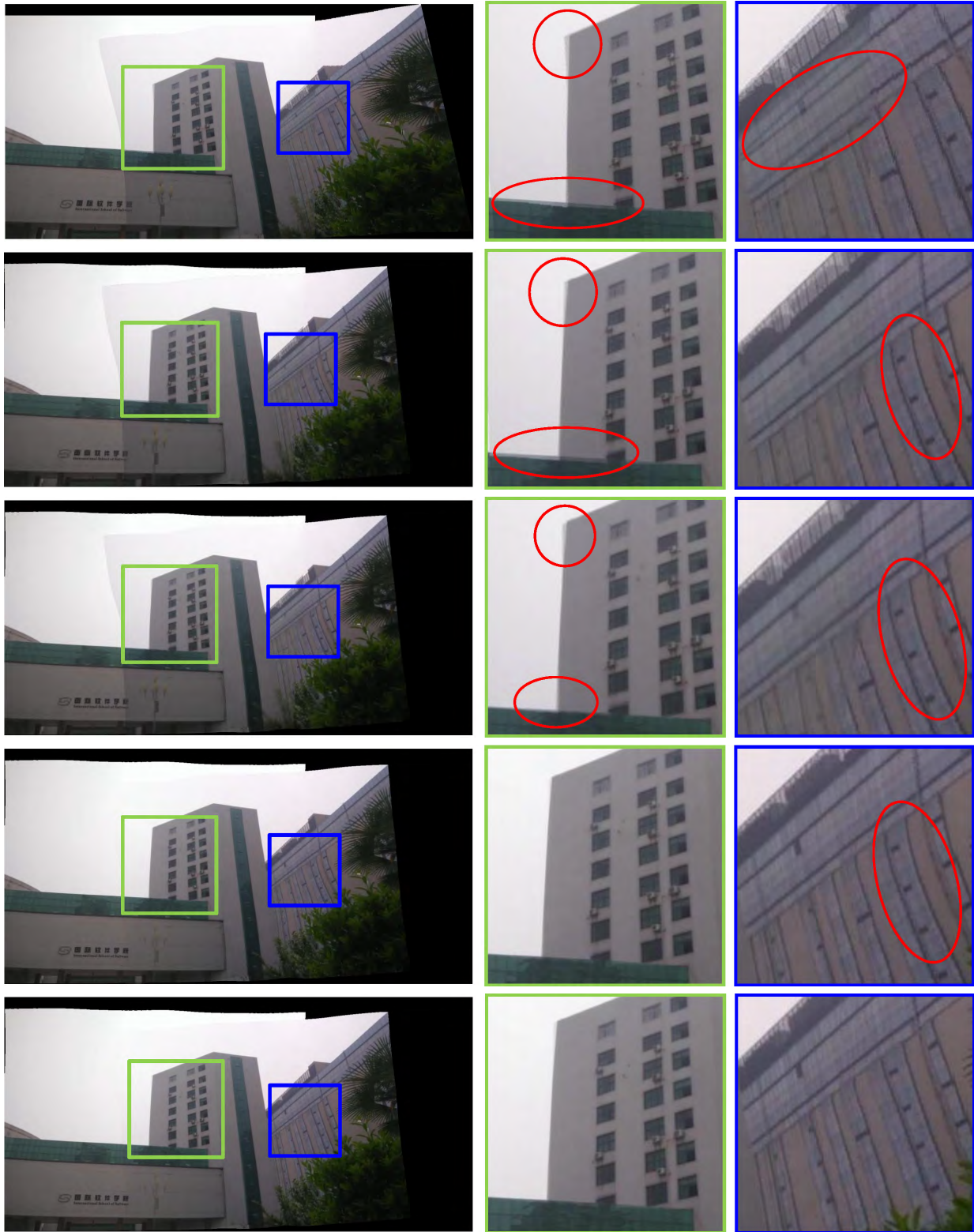


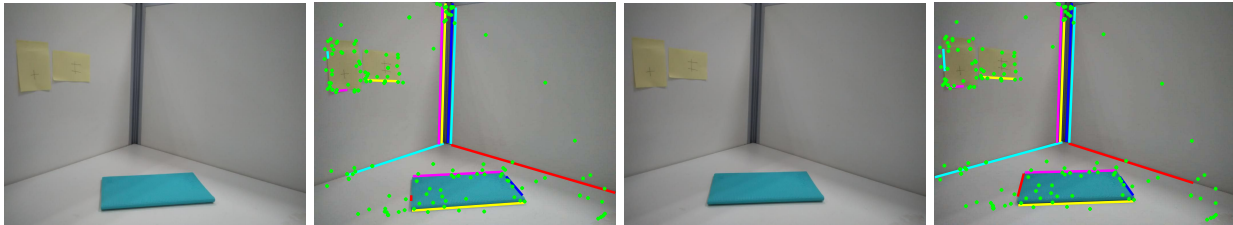
Figure 8: Performance of each constraint in proposed method on *School*. From top to bottom: (a) APAP, (b) Line-guided APAP (LAPAP), (c) LAPAP+CPW, (d) LAPAP+CPW+LineCorr, (e) Our method. Red circles show errors or distortions.

Table 1: Comparison of constraints on *School*

Methods	APAP	LAPAP	LAPAP+CPW	Proposed
Cor	1.024	0.730	0.666	0.664
Err_{mg}	2.766	2.099	1.785	1.708

tools for image stitching) by inputting two images at once. The final post-processed results are used since the original alignment results are not obtainable in the standard version of ICE. The quantitative comparison of ICE are also not given.

Fig. 9 shows the *Desk* image pair and the detected feature. For most low-textured areas, the key-points are difficult to be extracted, which results in insufficient matching points for the estimation of warping model. Line features can be used as an effective complement for alignment.

Figure 9: The *Desk* image pair for the assessment of image alignment.

The comparison results are given in Fig. 10. For the violation of the assumptions, the baseline warp is unable to align the images, and produces obvious misalignments (red boxes in Fig. 10(a)). ICE, CPW, APAP can provide relatively better stitching results, but ghost artifacts remain non-negligible. From Fig. 10(b), although ICE uses blending and pixel selection to conceal the misalignments, it is clear that the post-processing is not completely successful, for instance, the misalignments on vertical edge of the desk are obvious. Due to the insufficient corresponding key-points along the vertical edge of the desk, CPW and APAP cannot provide an accurate warping model for image alignment, so ghosting occurs in these regions (red boxes in Fig. 10(c)(d)). With the help of line correspondences and the two-stage robust alignment scheme, our method provides satisfactory stitching performance with accurate alignment and few ghost artefacts (Fig. 10(e)). It can be also found that our method reduces dependency on post-processing.

Table 2 depicts the Cor and Err_{mg} of the compared methods on *Desk* image pairs. As we can see, owing to the stronger constraint on point correspondences, CPW provides smaller alignment error on point $Err_{mg}^{(p)}$. But the alignment errors on line $Err_{mg}^{(l)}$ and Err_{mg} remain large. The proposed method achieves lower geometric error and yields better accuracy than other methods.

Table 2: Comparison of alignment on *Desk*

Methods	Cor	$Err_{mg}^{(p)}$	$Err_{mg}^{(l)}$	Err_{mg}
Baseline	0.390	4.894	5.632	5.001
CPW	0.299	1.534	3.703	1.849
APAP	0.360	2.652	4.407	2.907
Proposed	0.169	1.562	0.594	1.422

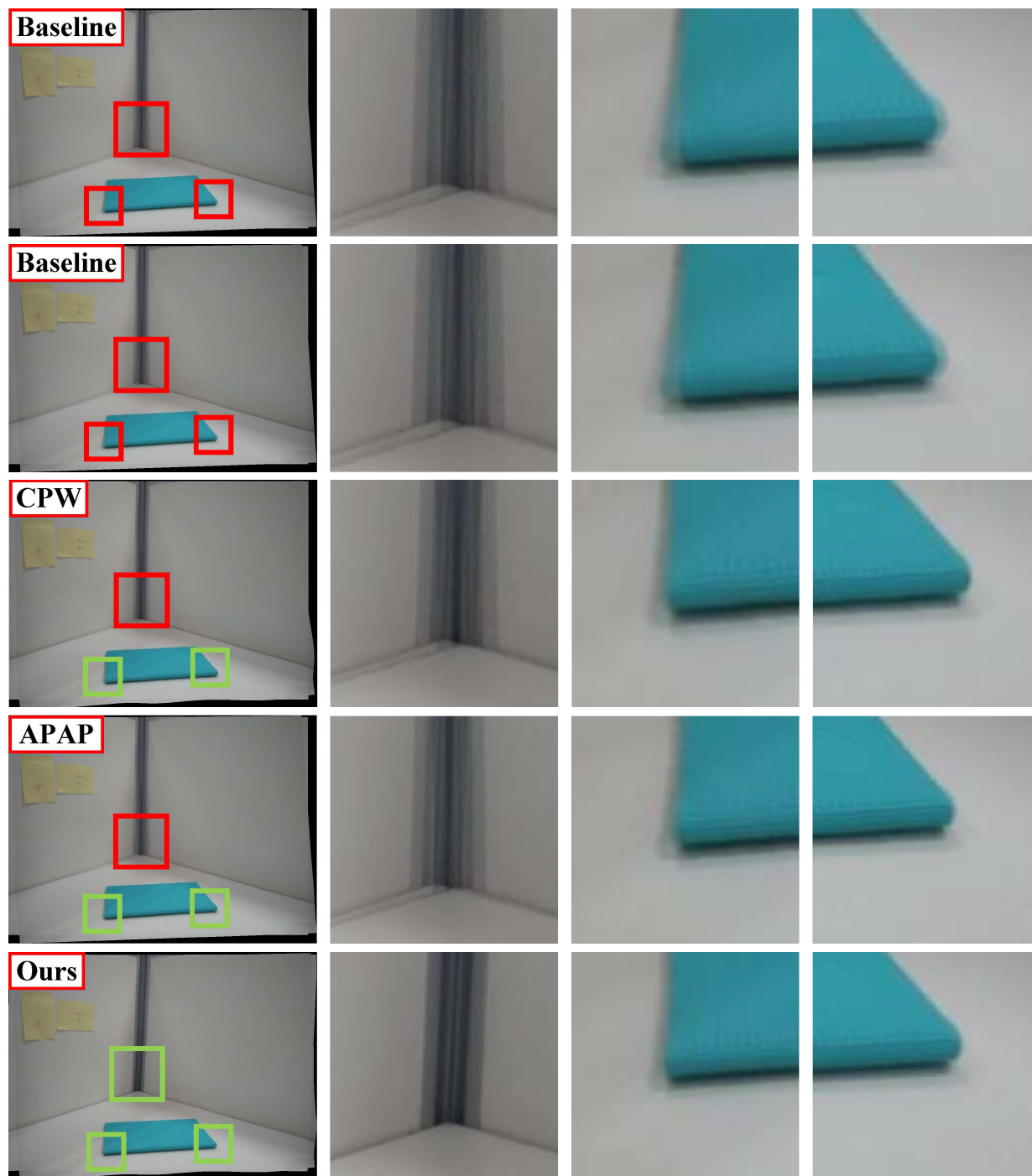


Figure 10: Comparison of image alignment for stitching on *Desk*. From top to bottom, the results are: (a) Baseline [12], (b) ICE [35], (c) CPW [10], (d) APAP [5], (e) our method. For better comparison, some details are highlighted. Red boxes show errors, green boxes show the satisfactory stitching.

4.2 Distortion reduction

To demonstrate the performance of distortion reduction, SPHP [11] and AANAP [15] have been compared on *Railtracks* and *Temple Square* images¹.



Figure 11: Comparison with SPHP method on distortion reduction. From top to bottom, the results are: (a) APAP [5], (b) SPHP0 [11], (c) SPHP1 [11], (d) our method. For better comparison, some details are highlighted.

¹*Railtracks* and *Temple Square* images come from the open dataset of [5].

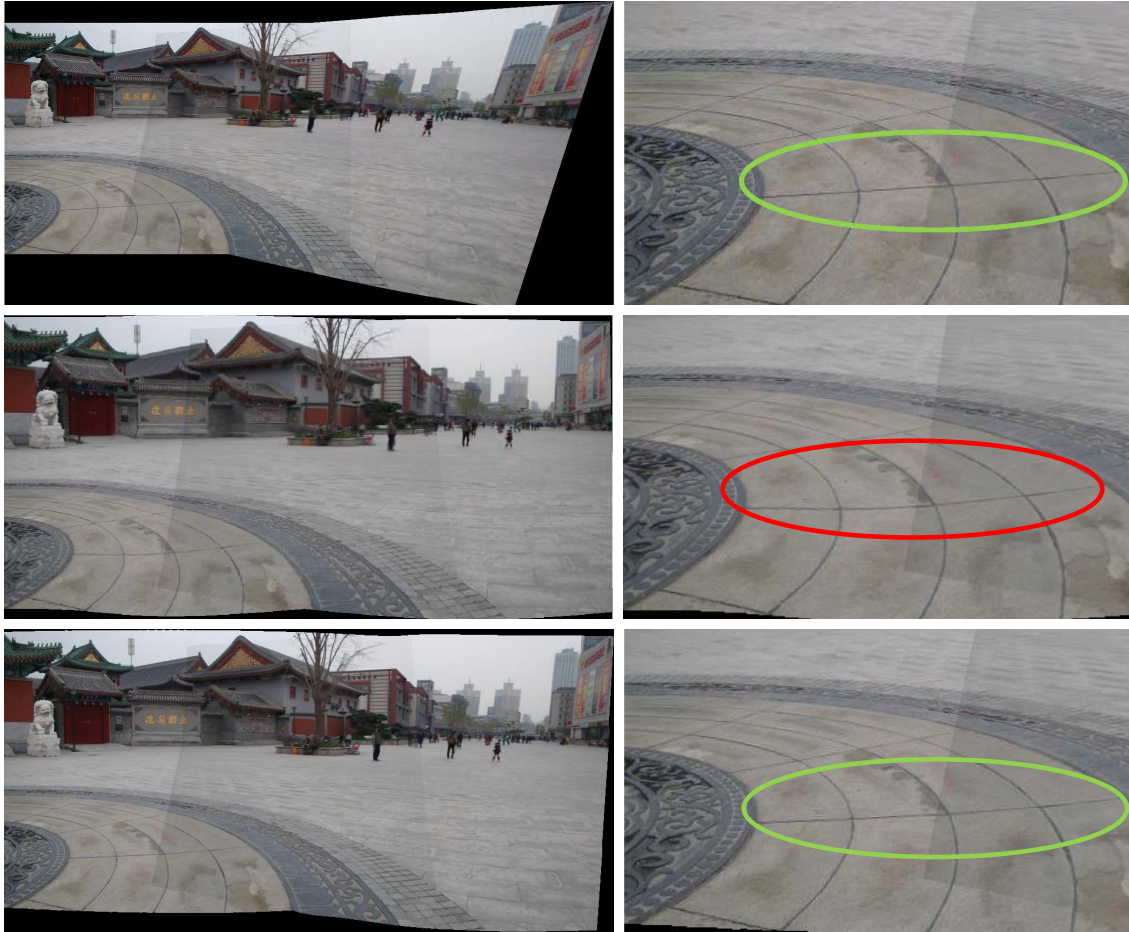


Figure 12: Comparison with AANAP method on distortion reduction. From top to bottom, the results are: (a) APAP [5], (b) AANAP [15], (c) our method. For better comparison, some details are highlighted. The red circle shows the distortion.

Fig. 11 shows the results of APAP [5], SPHP that restricts the similarity warp with rotation (SPHP0) [11], SPHP that restricts the similarity warp with no rotation (SPHP1) [11], and our method. Due to the simple extrapolation of projective transformation to non-overlapping regions, the result of APAP (Fig. 11(a)) shows projective distortions in the non-overlapping regions. Observing the closeup of blue box, the car is enlarged and the palm tree is obvious inclined. Introducing the similarity transformation, SPHP can largely mitigate the projective distortions. In Fig. 11(b), SPHP0 preserves the shape of car, but it has the problem with unnatural rotation. In addition, the construction site in red box is tilted to the left. SPHP1 preserves the shape and reduces the perspective distortion, but the construction site is slightly tilted to the right (11(c)). By our weight integration with similarity transformation, our method provides pleasing stitching result with less distortions in this example (11(d)).

Fig. 12 compares the proposed method with AANAP [15] on distortion reduction. Fig. 12(a) shows the good alignment of APAP, but it suffers from the problems of shape and perspective distortions, *e.g.* the stretched and tilted buildings in the right of image. Through linearizing homography and similarity transformation, AANAP provides an attractive result which the projective distortions have been largely

mitigated (Fig. 12(b)). However, as shown in the red circle of enlarged view, the lines on ground are slightly deformed. Our method gives more appealing stitching result in this example (Fig. 12(c)).

4.3 Comparisons with global-based methods

In this section, the proposed method is compared with the global-based methods, including global homography (Baseline) [12], ICE [35], SPHP [11]. For our method, the global homography is adopted in the first-stage of alignment and jointly estimated by point and line correspondences to pre-warp the source images, called global version.

Fig. 13 shows the two pairs of original images for stitching: *Ceiling* and *Temple*². From feature detection, because of the low-textured content of *Ceiling*, the number of detected key-points is limited, which making it challengeable for the accurate estimation of warping model. Despite *Temple* provides more rich point correspondences, the complex structure and the different imaging view remain a challenge for the global-based methods.



Figure 13: The original images for global-based methods. Top: *Ceiling*, bottom: *Temple*.

Fig. 14 and 15 show the results of global-based methods on *Ceiling* and *Temple* image pairs. As can be seen, for the model deficiency, the baseline warp cannot provide a satisfactory stitching results, getting into trouble of misalignments and projective distortions. ICE and SPHP improve the performance of stitching, especially in the aspect of the reduction of projective distortions, for instance, the door in Fig. 14 and the people in Fig. 15 suffer from less distortions, but the bricks of ceiling in the non-overlapping in ICE result (Fig. 14 (b)) remain to be slightly stretched. In addition, alignment errors in these two pair of images (red circles in Fig. 14 and 15) remain obvious. In contrast, the proposed method is not only more flexible and robust to handle the alignment because of the line-guided warping estimation, but also because of the alignment constraints in the mesh-based framework. With similarity constraint, our method provides good stitching results with minimal distortions.

Table 3 and Table 4 gives the quantitative comparison of *Ceiling* and *Temple*. It can be seen that our method provides the results with least errors. As for *Ceiling*, our method performs the best as the line feature play an important role in such scenes without reliable key-point correspondences. For *Temple* with rich reliable key-points, the role of line feature may be reduced, but it still helps to improve the accuracy of alignment.

² *Temple* images come from the open dataset of [5].

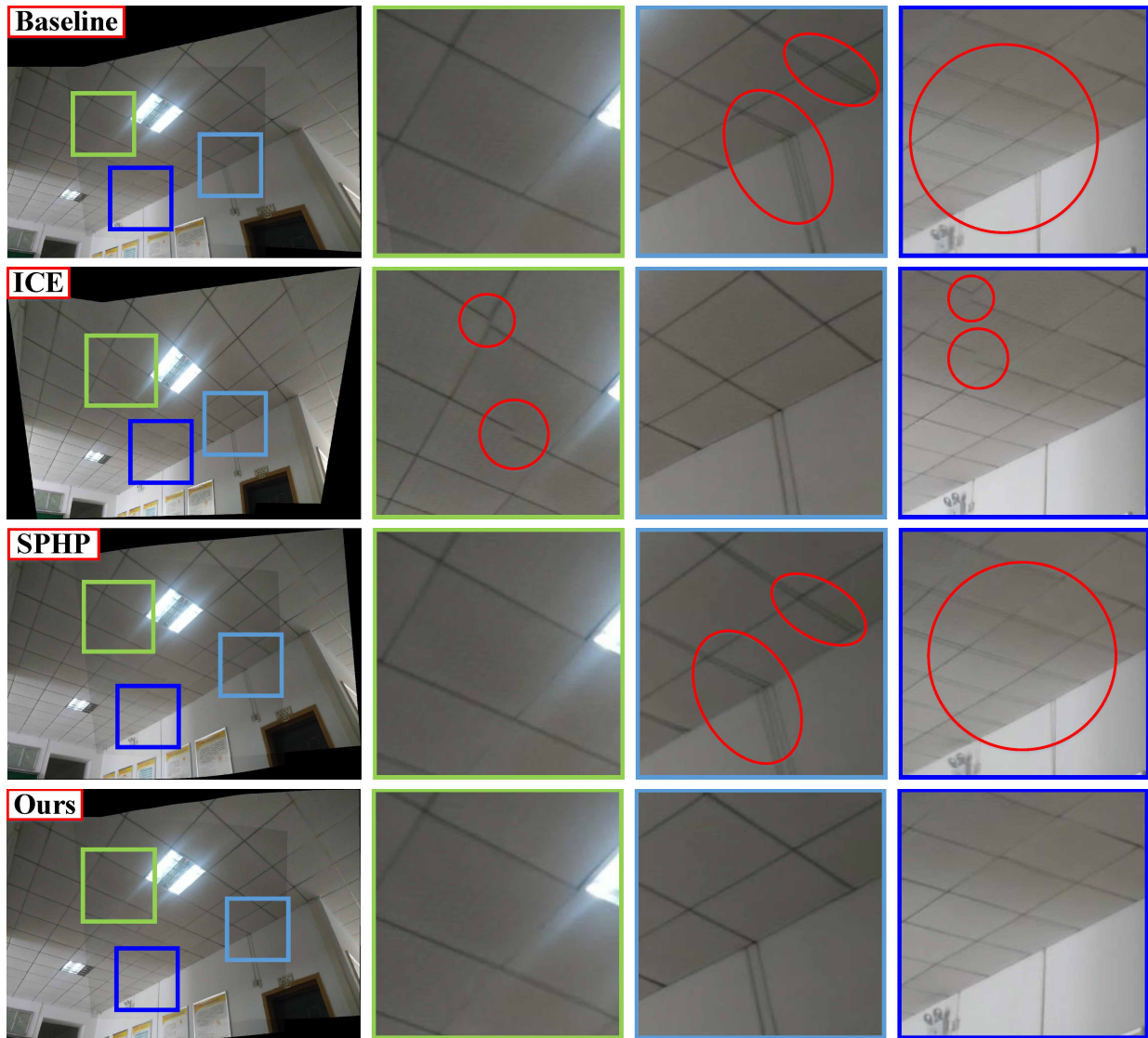


Figure 14: Comparison of image stitching on *Ceiling*. From top to bottom, the results are: (a) Baseline [12], (b) ICE [35], (c) SPHP [11], (d) our method (global version). For better comparison, some details are highlighted. The red circles show alignment errors.

Methods	Cor	$Err_{mg}^{(p)}$	$Err_{mg}^{(l)}$	Err_{mg}
Baseline	0.755	3.200	2.059	2.452
SPHP	0.631	2.876	1.989	2.292
Proposed	0.200	1.343	0.695	0.921

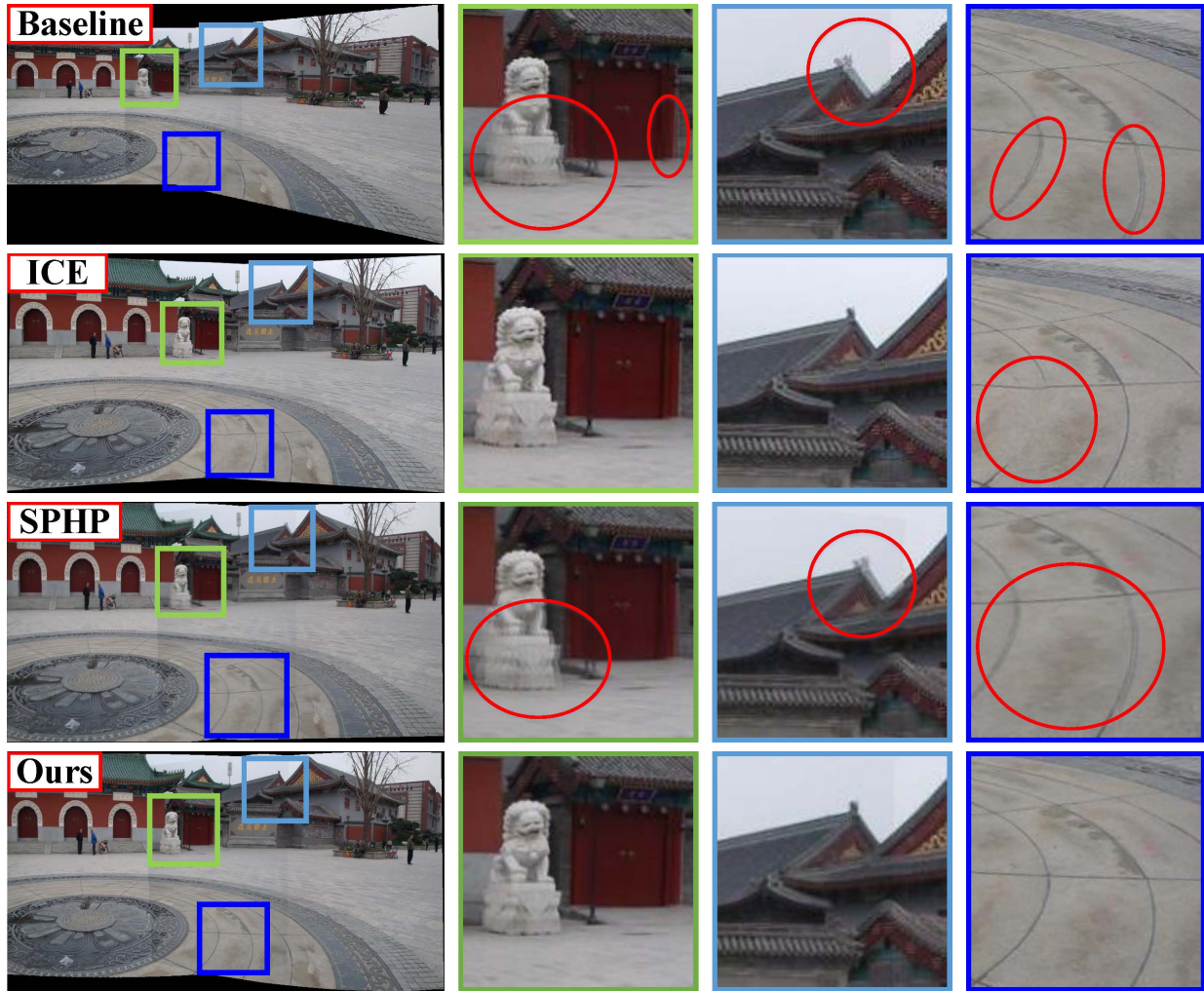


Figure 15: Comparison of image stitching on *Temple*. From top to bottom, the results are: (a) Baseline [12], (b) ICE [35], (c) SPHP [11], and (d) our method (global version). For better comparison, some details are highlighted. The red circles show alignment errors.

Methods	Cor	$Err_{mg}^{(p)}$	$Err_{mg}^{(l)}$	Err_{mg}
Baseline	6.240	1.899	0.954	1.430
SPHP	4.334	1.756	0.919	1.341
Proposed	1.515	0.592	0.529	0.561

4.4 Comparisons with local-based methods

The global version works well in preserving the content and perspective, but it maybe a little helpless on alignment when images are taken with large views. For high DOFs and flexible local homographies, our method with local homography in pre-warping stage (called local version) can handle parallax issue, so it is compared with other local-based methods in this section, including CPW [10], APAP [5], SPHP+APAP [11]. Fig. 16 illustrates the original images for compared experiments: *Church*, *Block*, and *Wall* images³. Some images are low-textured and the extracted features are limited. Moreover, the images' corresponding views vary greatly.

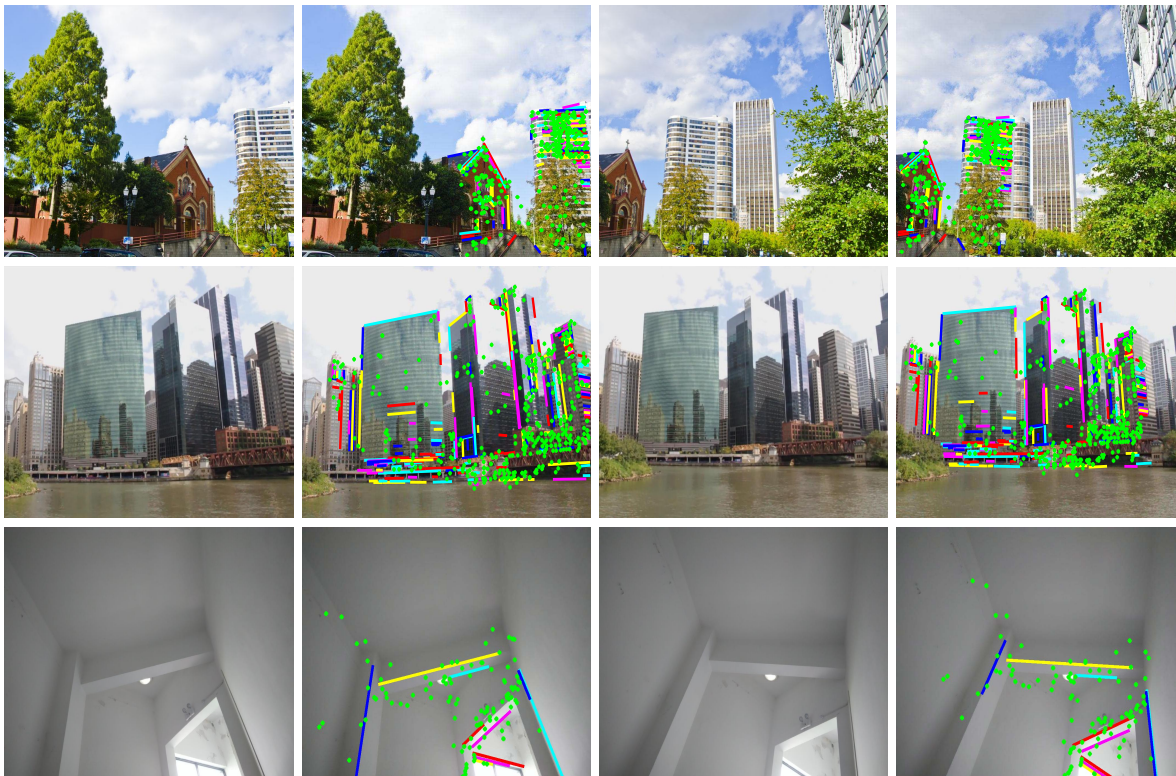


Figure 16: The original images for comparison of local-based methods. From top to bottom, they are: *Church*, *Block*, and *Wall*.

The stitching results on these three pairs of images are provided in Fig. 17. In terms of alignment accuracy, CPW and APAP allows higher DoFs than global homography, but they also produce misalignments at the regions where lack of point correspondences (partially highlighted in red boxes). Except that, CPW and APAP may cause local structure deformation on structural regions where lack of key-points, such as stair railing in *Church* (the left red boxes in Fig. 17 (a)), the building boundary in *Block* (the bottom red boxes), the wall boundary in *Wall* (the left red boxes), where the lines become curved. With the similarity transformation, SPHP+APAP can reduce the projective distortions and preserve the shape and perspective, shown in *Church* and *Block*, where the distortions of buildings in the right are mitigated. In contrast, our method can not only provide accurate alignment which benefits from the two-stage alignment scheme, but also preserve image structure and perspective for the line and similarity constraints.

³*Church* and *Block* iamges come from the open dataset of [3].

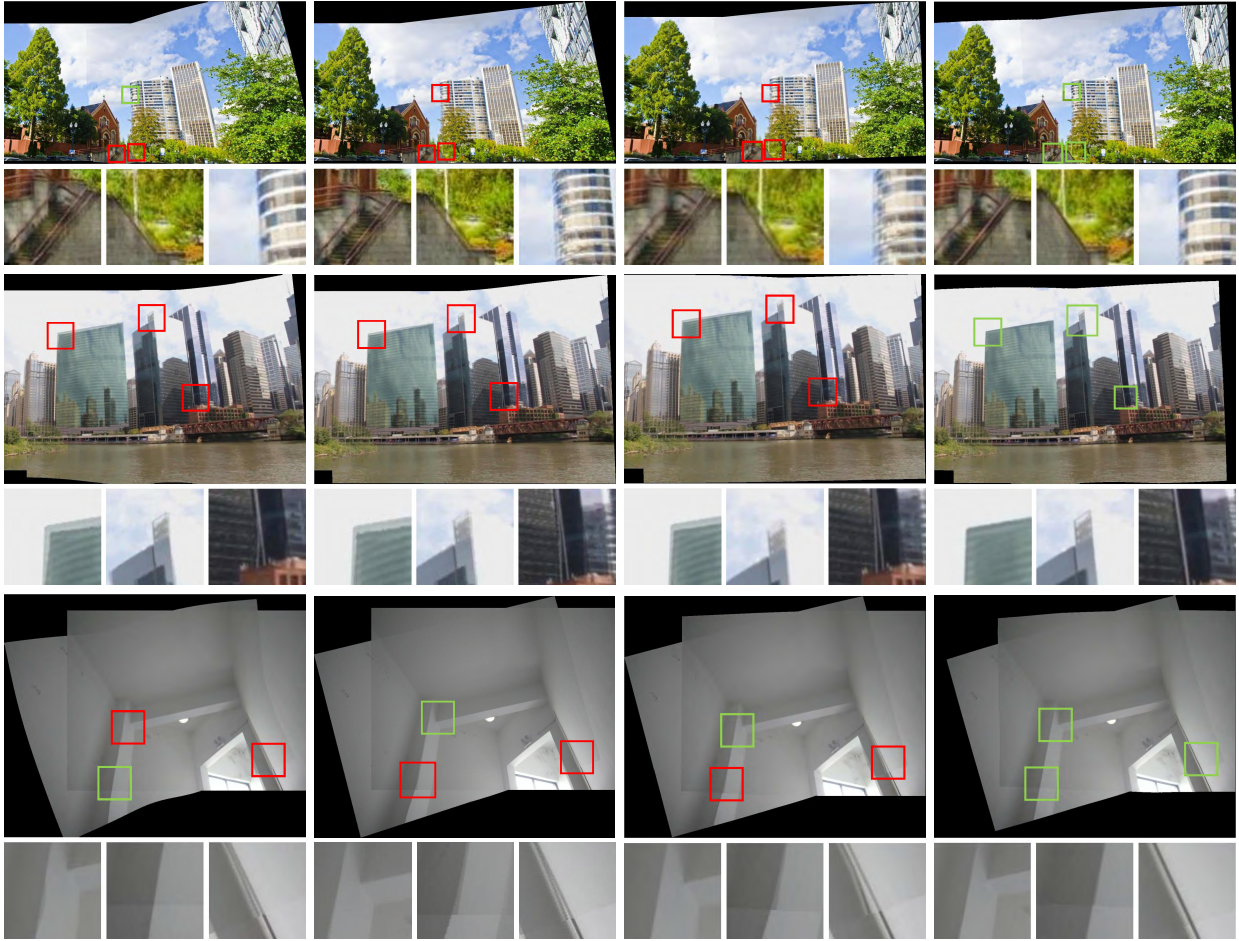


Figure 17: Comparison of image stitching on *Church*, *Block*, and *Wall*. From left to right, the results are: (a) CPW [10], (b) APAP [5], (c) SPHP+APAP [11], (d) our method (local version). For better comparison, the details are highlighted. Red boxes show alignment errors or distortions, green boxes show the satisfactory stitching. The enlarged views are displayed below each image stitching result.

Table 5 shows the quantitative results of compared methods. Our method consistently yields better accuracy than CPW, APAP and SPHP+APAP except for $Err_{mg}^{(p)}$ in *Church* result. CPW adopts the feature alignment as a strong constraint, so it provides good quantitative result in $Err_{mg}^{(p)}$. But it provides unsatisfactory result in other criteria in *Church* result. As a whole, our method provides the best quantitative results.

Table 5: Quantitative Evaluation of local-based methods

Methods	<i>Church</i>				<i>Block</i>				<i>Wall</i>			
	<i>Cor</i>	$Err_{mg}^{(p)}$	$Err_{mg}^{(l)}$	Err_{mg}	<i>Cor</i>	$Err_{mg}^{(p)}$	$Err_{mg}^{(l)}$	Err_{mg}	<i>Cor</i>	$Err_{mg}^{(p)}$	$Err_{mg}^{(l)}$	Err_{mg}
CPW	4.950	0.599	0.876	0.686	2.561	1.600	1.582	1.592	0.308	2.348	2.100	2.312
APAP	6.485	1.319	1.261	1.300	3.013	2.719	1.710	2.263	0.252	3.490	2.178	3.302
SPHP+APAP	4.281	1.310	1.280	1.301	2.849	2.668	1.651	2.208	0.198	3.498	2.249	3.318
Proposed	3.090	0.630	0.515	0.594	1.880	1.550	0.627	1.133	0.081	2.248	0.478	1.993

5 Conclusion

This paper proposes *a line-guided local warping for image stitching by imposing similarity constraint*. Our method integrates multiple constraints, including line feature constraints and global similarity constraint, into a two-stage image stitching framework, which achieves accurate alignment and also mitigate distortions. The line feature is employed as an effective complement to the point feature for alignment. Then the line feature constraints, line matching and line collinearity, are integrated into the mesh-based warping framework, aiming to further improve the alignment while preserving the image structures. Additionally, the global similarity transformation is combined with the projective warping to maintain the image content and perspective. From the experiments, a good image stitching with least alignment errors and distortions is achieved by the proposed method.

References

- [1] S. Pang, M. Sun, X. Hu, and Z. Zhang, “Sgm-based seamline determination for urban orthophoto mosaicking,” *ISPRS J PHOTOGRAMM*, vol. 112, pp. 1–12, 2016.
- [2] X. Li, N. Hui, H. Shen, Y. Fu, and L. Zhang, “A robust mosaicking procedure for high spatial resolution remote sensing images,” *ISPRS J PHOTOGRAMM*, vol. 109, pp. 108–125, 2015.
- [3] Y. Zhang, S. Song, P. Tan, and J. Xiao, “Panocontext: A whole-room 3d context model for panoramic scene understanding,” in *ECCV*, 2014, pp. 668–686.
- [4] Brown and Lowe, “Recognising panoramas,” in *ICCV*, 2003, pp. 1218–1225.
- [5] J. H. Zaragoza, T. Chin, Q. Tran, M. S. Brown, and D. Suter, “As-projective-as-possible image stitching with moving dlt,” *IEEE Trans. PAMI*, vol. 36, no. 7, pp. 1285–1298, 2014.
- [6] J. Gao, Y. Li, T. J. Chin, and M. S. Brown, “Seam-driven image stitching,” in *Eurographics*, 2013, pp. 45–48.
- [7] W. Wang and M. K. Ng, “A variational method for multiple-image blending,” *IEEE Trans. IP*, vol. 21, no. 4, pp. 1809–1822, 2011.
- [8] J. Hu, D. Q. Zhang, H. Yu, and C. W. Chen, “Multi-objective content preserving warping for image stitching,” in *ICME*, 2015, pp. 1–6.

- [9] R. Szeliski, “Image alignment and stitching: a tutorial,” *Foundations and Trends in Computer Graphics and Vision*, vol. 2, no. 1, pp. 1–104, 2006.
- [10] F. Liu, M. Gleicher, H. Jin, and A. Agarwala, “Content-preserving warps for 3d video stabilization,” *ACM Trans. GRAPHIC*, vol. 28, no. 3, p. 44, 2009.
- [11] C. H. Chang, Y. Sato, and Y. Y. Chuang, “Shape-preserving half-projective warps for image stitching,” in *CVPR*, 2014, pp. 3254–3261.
- [12] M. Brown and D. G. Lowe, “Automatic panoramic image stitching using invariant features,” *INT J COMPUT VISION*, vol. 74, no. 1, pp. 59–73, 2007.
- [13] K. Joo, N. Kim, T. H. Oh, and I. S. Kweon, “Line meets as-projective-as-possible image stitching with moving dlt,” in *ICIP*, 2015, pp. 1175–1179.
- [14] S. Li, L. Yuan, J. Sun, and L. Quan, “Dual-feature warping-based motion model estimation,” in *ICCV*, 2015, pp. 4283–4291.
- [15] C. C. Lin, S. U. Pankanti, K. N. Ramamurthy, and A. Y. Aravkin, “Adaptive as-natural-as-possible image stitching,” in *CVPR*, 2015, pp. 1155–1163.
- [16] G. S. Xia, J. Delon, and Y. Gousseau, “Accurate junction detection and characterization in natural images,” *INT J COMPUT VISION*, vol. 106, no. 1, pp. 31–56, 2014.
- [17] T. Xiang, G. S. Xia, and L. Zhang, “Locally warping-based image stitching by imposing line constraints,” in *ICPR*, 2016.
- [18] J. Gao, S. J. Kim, and M. S. Brown, “Constructing image panoramas using dual-homography warping,” in *CVPR*, 2011, pp. 49–56.
- [19] W. Y. Lin, S. Liu, Y. Matsushita, T. T. Ng, and L. F. Cheong, “Smoothly varying affine stitching,” in *CVPR*, 2011, pp. 345–352.
- [20] R. Hartley and A. Zisserman, *Multiple view geometry in computer vision*. Cambridge University Press, 2003.
- [21] E. Dubrofsky and R. J. Woodham, “Combining line and point correspondences for homography estimation,” in *ISVC*, 2008, pp. 202–213.
- [22] F. Zhang and F. Liu, “Parallax-tolerant image stitching,” in *CVPR*, 2014, pp. 3262–3269.
- [23] C.-H. Chang, C.-J. Chen, and Y.-Y. Chuang, “Spatially-varying image warps for scene alignment,” in *ICPR*, 2014, pp. 64–69.
- [24] Y.-S. Chen and Y.-Y. Chuang, “Natural image stitching with the global similarity prior,” in *ECCV*, 2016, pp. 186–201.
- [25] P. S. Heckbert, *Fundamentals of texture mapping and image warping*. University of California, Berkeley, 1989.
- [26] T. J. Chin, J. Yu, and D. Suter, “Accelerated hypothesis generation for multistructure data via preference analysis,” *IEEE Trans. PAMI*, vol. 34, no. 4, pp. 625–638, 2012.
- [27] T. Xiang, G. Xia, and L. Zhang, “Image stitching with perspective-preserving warping,” in *XXIII ISPRS Congress*, 2016.

- [28] O. Chum, T. Pajdla, and P. Sturm, “The geometric error for homographies,” *COMPUT VIS IMAGE UND*, vol. 97, no. 1, pp. 86–102, 2005.
- [29] O. Chum and J. Matas, “Planar affine rectification from change of scale,” in *ACCV*, 2010, pp. 347–360.
- [30] D. G. Lowe, “Distinctive image features from scale-invariant keypoints,” *INT J COMPUT VISION*, vol. 60, no. 2, pp. 91–110, 2004.
- [31] A. Vedaldi and B. Fulkerson, “Vlfeat: An open and portable library of computer vision algorithms,” in *ACMMM*, 2010, pp. 1469–1472.
- [32] R. G. von Gioi, J. Jakubowicz, J.-M. Morel, and G. Randall, “Lsd: A fast line segment detector with a false detection control,” *IEEE Trans. PAMI*, vol. 32, no. 4, pp. 722–732, 2010.
- [33] B. Fan, F. Wu, and Z. Hu, “Robust line matching through line-point invariants,” *Pattern Recognition*, vol. 45, no. 2, pp. 794–805, 2012.
- [34] K. Li, J. Yao, X. Lu, L. Li, and Z. Zhang, “Hierarchical line matching based on linejunctionline structure descriptor and local homography estimation,” *Neurocomputing*, vol. 184, pp. 207–220, 2016.
- [35] “Microsoft research, image composite editor,” pp. <http://research.microsoft.com/en-us/um/redmond/projects/ice/>, 2015.